NACA

RESEARCH MEMORANDUM

AERODYNAMICS OF SLENDER BODIES AT MACH NUMBER OF 3.12 AND

REYNOLDS NUMBERS FROM 2×10^6 TO 15×10^6

II – AERODYNAMIC LOAD DISTRIBUTIONS OF SERIES OF FIVE BODIES

HAVING CONICAL NOSES AND CYLINDRICAL AFTERBODIES

By John R. Jack and Lawrence I. Gould

Lewis Flight Propulsion Laboratory
Cleveland, Ohio

NATIONAL ADVISORY COMMITTEE
FOR AERONAUTICS
WASHINGTON
May 8, 1952

2434

NATIONAL ADVISORY COMMITTEE FOR AERONAUTICS

RESEARCH MEMORANDUM

AERODYNAMICS OF SLENDER BODIES AT MACH NUMBER OF 3.12

AND REYNOLDS NUMBERS FROM 2X10^6 TO 15X10^6

II - AERODYNAMIC LOAD DISTRIBUTIONS OF SERIES OF

FIVE BODIES HAVING CONICAL NOSES AND

CYLINDRICAL AFTERBODIES

By John R. Jack and Lawrence I. Gould

SUMMARY

An experimental investigation to determine the aerodynamic load distributions of a series of five bodies having conical or slightly blunted noses and cylindrical afterbodies was conducted in the NACA Lewis 1- by 1-foot supersonic wind tunnel. Pressure distributions and viscous drags were measured at a Mach number of 3.12 for a Reynolds number range of 2X10^6 to 14X10^6 and for an angle of attack range of 0° to 9°.

For zero angle of attack and a Reynolds number range of 2X10^6 to 14X10^6, linearized potential theory predicted the pressure distributions satisfactorily for all pointed bodies having large nose fineness ratios. The exact conical flow theory predicted the cone surface pressures well regardless of nose fineness ratio. At small angles of attack, the experimental pressure distributions due to angle of attack on the top and the bottom surfaces of a representative model agreed fairly well with slender-body theory for all Reynolds numbers. The theoretical data obtained from Massachusetts Institute of Technology tables predicted the conical pressures well for all angles of attack.

The base-pressure coefficient for the higher Reynolds numbers decreased uniformly as the angle of attack was increased; for the low Reynolds number, however, the base-pressure coefficient increased and then decreased as the angle of attack increased. The maximum base-pressure coefficient was obtained at angles of attack of about ±3°. For the five models investigated at a Reynolds number of 14X10^6, the base-pressure coefficient did not vary more than ±4 percent from a median curve.

A summation of the drag components for zero angle of attack showed that the total-drag coefficient for free transition increased with increasing Reynolds number until some Reynolds number between 2×10^6 and 8×10^6 was reached. Further increases in Reynolds number had no appreciable effect on the total-drag coefficient.

INTRODUCTION

The investigation reported herein is the second of a series conducted in the NACA Lewis 1- by 1-foot supersonic wind tunnel to extend the basic information on the aerodynamics of bodies of revolution with varying Reynolds numbers and to evaluate the validity of several theories for predicting the pressures acting on such bodies. The first of this series of investigations was reported in reference 1, which contains an evaluation of the aerodynamics of a near-parabolic nose body. The subject of the present report is the aerodynamic load distributions obtained with a series of five bodies having conical or slightly blunted noses and cylindrical afterbodies at a Mach number of 3.12 for Reynolds numbers from 2×10^6 to 14×10^6 and for angles of attack from 0° to 9°.

Pressure distributions were obtained for all models at a Reynolds number of 14×10^6 and at Reynolds numbers of 2×10^6 and 8×10^6 for a representative model. These experimentally determined pressure coefficients are compared with several theories. In order to obtain the over-all drag of the representative model, a momentum survey was made at the base of the model for natural transition and for forced transition.

SYMBOLS

The following symbols are used in this report:

A_F frontal area

C_D drag coefficient, $D/q_0 A_F$

C_p pressure coefficient, $(p-p_0)/q_0$

D drag

d maximum body diameter

l body length

M_0 free-stream Mach number

2434

p   static pressure

q_0 free-stream dynamic pressure, $(\gamma/2)\, p_0 M_0{}^2$

Re   Reynolds number, $\rho_0 U_0 l/\mu$

U_0 free-stream velocity

u   velocity in boundary layer

x,r,θ cylindrical coordinates

α angle of attack

γ ratio of specific heats, 1.40

θ momentum thickness, $\dfrac{1}{\rho_1 u_1{}^2} \displaystyle\int_0^{\infty} \rho u (u_1 - u)\ dy$

μ viscosity

ρ density

ϕ perturbation-velocity potential

Subscripts:

0   free-stream conditions

1   conditions at edge of boundary layer

b   base

f   friction

p   pressure

APPARATUS AND PROCEDURE

The investigation was conducted in the Lewis 1- by 1-foot vari-able Reynolds number tunnel, which is a nonreturn-type tunnel with a test-section Mach number of 3.12 ±0.03. A stagnation temperature of approximately 60° F was maintained throughout the investigation, and inlet pressures were varied from 7 to 50 pounds per square inch

absolute. The entering air had a specific humidity of approximately 2×10^{-5} pounds of water per pound of dry air, which insured negligible condensation effects.

A schematic diagram with pertinent dimensions of each model is presented in figure 1. All models were machined from mild steel and polished to a 16-microinch finish. The static-pressure orifices on the models were arranged in five rows and were located at stations given in table I. Each model base had four static-pressure orifices located in one quadrant 30° apart. The momentum survey at the base of the representative model (model 2, fig. 1) was made for free transition and forced transition with the probe pictured in figure 2. A wire ring made from 0.010-inch-diameter copper wire and placed 0.675 inch downstream of the tip of the model was used for forcing transition.

The models were supported by a sting extending upstream from a horizontal strut mounted to the side of the tunnel (fig. 3). Interference of the sting with the base pressures at zero angle of attack was minimized by designing the sting on the basis of the data presented in reference 2. Angle of attack was varied by rotating each model about a point 4 inches upstream of the base.

REDUCTION OF DATA AND METHOD OF COMPUTATION

In the reduction of the pressure data, the free-stream static pressure was assumed to be the static pressure measured on the tunnel wall opposite the model tip. The incremental pressure coefficients due to angle of attack $C_{p,\alpha}$ were obtained by subtracting the values measured at zero angle of attack from those measured at angle of attack.

The boundary-layer-survey data obtained at the base of the representative model were evaluated by the Rankine-Hugoniot equation with the assumption that the total temperature was constant in the flow field, and that the static pressure was constant along radial lines through the boundary layer. Skin-friction coefficients were obtained by calculating the momentum loss at the base of the representative model. The effect of body pressure gradient on the calculated skin-friction drag was not considered because this effect is shown to be negligible in reference 3.

The theoretical pressure-distribution curves were calculated from the following equations (reference 4):

$$C_p = -\frac{2}{U_0}\left(\frac{\partial \phi}{\partial x}\right)_{\alpha=0} - \left(\frac{dr}{dx}\right)^2 \tag{1}$$

$$C_{p,\alpha} = 4\alpha \cos \theta \frac{dr}{dx} + \alpha^2(1 - 4 \sin^2 \theta) \qquad (2)$$

where $\left(\frac{\partial \phi}{\partial x}\right)_{\alpha=0}$ is the axial perturbation velocity associated with zero angle of attack. The perturbation velocities for zero angle of attack were computed using the numerical method of reference 5. In the vicinity of a discontinuity in surface slope, the linearized potential theory is not expected to be valid.

RESULTS AND DISCUSSION

The experimental results consist of pressure distributions on the forebodies and the afterbodies of all the models of figure 1 for angles of attack from 0° to 9°. In addition, the boundary layer at the base station of model 2 was surveyed for four Reynolds numbers at zero angle of attack. The results for zero angle of attack are discussed for all models; however, because the effects of angle of attack are approximately the same for all models, only these effects for a representative model (model 2) are discussed.

Zero Angle of Attack

The experimental variation of the pressure coefficient with axial position for a Reynolds number of 14×10^6 is presented in figure 4 for models 1, 2, and 3. Theoretical curves computed from the linearized potential theory and the exact conical flow theory are compared with the experimental data. For small cone angles, the second-order theory of reference 6 agrees very well with the exact conical theory; consequently, the experimental data for zero angle of attack has not been compared with the second-order theory. The qualitative agreement between experiment and linearized potential theory is good except for model 1 (fig. 4(a)) for which the theoretical prediction for the cone is approximately 30 percent lower than a median line through the experimental data. This is to be expected, however, since the cone half-angle is large (10°). Agreement with the exact conical values is good.

The experimental variation of pressure coefficient with axial station for model 2 is presented in figure 5 for Reynolds numbers of 2×10^6, 8×10^6, and 14×10^6. Agreement between experiment, the exact conical theory, and the linearized potential theory is good for the Reynolds number range investigated. One interesting point was revealed by the low Reynolds number investigation. Originally, the model was instrumented with 0.035-inch-inside-diameter tubing, which measured a pressure

that gave a cone pressure coefficient approximately 1.5 times as great as theory. By using 0.048-inch-inside-diameter tubing, however, the measured data were found to be in good agreement with theory and the experimental data at the higher Reynolds numbers (fig. 5(a)). A preliminary investigation indicated that this phenomenon is a result of the diffusion of atmospheric air through the flexible plastic tubing used in the manometer system. The data obtained from the 0.048-inch-inside-diameter tubing has been used for all the low Reynolds number curves.

The distribution of pressure coefficients over the blunt, conical-nosed models 4 and 5 for a Reynolds number of 14×10^6 is shown in figure 6. For both models, the pressure-coefficient distribution begins at the free-stream stagnation value, expands to a very low pressure coefficient, and subsequently recompresses to a value approximately equal to the exact conical value for a cone with a half-angle equal to the inclination of the straight portion of the nose.

The experimental and theoretical variation of pressure-fore-drag coefficient with nose fineness ratio for all bodies is shown in figure 7. The experimental pressure-drag coefficients represent an average of the $\theta = 0^{\circ}$ and the $\theta = 90^{\circ}$ data. Several conclusions may be drawn from figure 7, namely: (1) Agreement between experiment and linearized potential theory for the sharp-nosed bodies is good only at the higher nose fineness ratios; however, the exact conical theory is in good agreement with experiment for all nose fineness ratios; (2) For the same nose fineness ratio, the pressure-drag coefficients for the blunt-nosed models investigated are at least 2.5 times as large as those for the corresponding conical-nosed models. (A minimum and a maximum pressure-drag coefficient have been plotted in figure 7 for the blunt-nosed bodies to give an idea of the possible error in the experimental pressure-drag coefficient, because the instrumentation on the blunt part of the nose was probably insufficient to determine the pressure-drag coefficients accurately.) (3) The pressure-drag coefficient for the representative model changes very little with an increase in Reynolds number from 2×10^6 to 14×10^6.

In order to complete the investigation of the component drag forces which contribute to the total drag of model 2 at zero angle of attack, friction-drag coefficients were obtained from the experimentally determined momentum thicknesses at the base of the model for Reynolds numbers of 2×10^6, 4×10^6, 8×10^6, and 14×10^6. The experimental momentum thicknesses from which the skin-friction coefficients were calculated are presented in figure 8. It is evident from figure 8 that the 0.010-inch-diameter wire ring was unsuccessful in causing transition at a Reynolds number of 2×10^6. This conclusion is also substantiated by a comparison of the two velocity profiles. The experimental variation of total-drag coefficient with Reynolds number, obtained by

adding the component drag coefficients, is presented in figure 9. The curves are broken between the Reynolds numbers of 2×10^6 and 8×10^6 because of the uncertain variation of the component drag coefficients between these two Reynolds numbers. The total-drag coefficient for free and for forced transition increased with increasing Reynolds number until some Reynolds number between 2×10^6 and 8×10^6 was reached and then remained almost constant at a value of approximately 0.18. This type of variation of total-drag coefficient with Reynolds number was also observed in reference 1. Figure 9 also shows the variation of the base-pressure-drag coefficient with Reynolds number. This type of variation was observed in reference 1.

Angle of Attack

The axial pressure distributions along the bottom and the top of the representative model 2 are presented in figure 10 for two angles of attack and three Reynolds numbers. Angle-of-attack data for models 1, 3, 4, and 5 are presented in tables II, III, IV, and V, respectively, for a Reynolds number of 14×10^6. The pressure-coefficient increments due to angle of attack for model 2, as determined from figures 5 and 10, are compared in figure 11 with slender-body theory (equation (2)), the series solution of reference 6, and the theoretical data of reference 7.

For the bottom surface $(\theta = 0^{\circ})$ of the model nose, figure 11 shows that all three theories used for comparison are in good agreement with experiment for an angle of attack of 3°. However, at an angle of attack of 9° the second-order theory of reference 7 is in best agreement with experiment. The slender-body theory and the series-expansion solution of reference 6 are low, the series-expansion solution being appreciably lower than experiment. This difference might be expected, however, because the series-expansion solution of reference 6 is linearized with respect to angle of attack. On the top surface $(\theta = 180^{\circ})$ of the model nose, experiment and theory are again in good agreement for an angle of attack of 3°. For an angle of attack of 9° the slender-body theory agrees best with experiment. The series-expansion solution of reference 6 predicts a pressure coefficient too low, whereas the theoretical data of reference 7 give a pressure coefficient somewhat high. No significant Reynolds number effect was noticed for the Reynolds number range investigated. For the cylindrical portion of the body, experiment and slender-body theory are in fair agreement for an angle of attack of 3° $(\theta = 0^{\circ}$ and $180^{\circ})$ but not for an angle of attack of 9°. The discrepancy at the high angle of attack can be attributed to some extent to cross-flow separation.

The variation of the experimentally determined pressure coefficients with meridian angle around the body is given in figure 12 for three Reynolds numbers and for four axial stations, the first two of which are on the cone. Because the highest Reynolds number is of most practical interest, only the experimental pressure-coefficient increments due to angle of attack for a Reynolds number of 14×10^6 are compared with theory in figure 13. For an angle of attack of $3°$ and for the cone surface (fig. 13(a)), the agreement between experiment and the three theories used for comparison is good, although the theory of reference 6 overestimates the side pressures slightly. Slender-body theory also adequately predicts the pressures acting on the cylindrical surface at an angle of attack of $3°$. The pressures acting on the cone surface at an angle of attack of $9°$ are best predicted by slender-body theory and the second-order theory of reference 7. For an angle of attack of $9°$ and for the cylindrical surface (figs. 13(b) and 13(c)), experiment and slender-body theory are in fair agreement for the first quadrant, but marked deviations occur in the second quadrant. The differences between experiment and the theories used for comparison may be attributable to the inadequacy of the theories or to the effects of cross-flow separation, which are not considered in the theories.

The variation of the base-pressure coefficient with angle of attack for the representative model at three Reynolds numbers is presented in figure 14. The base-pressure coefficients for the higher Reynolds numbers decrease steadily as the angle of attack increases; for the low Reynolds number, however, the pressure coefficient first increases to a maximum near an angle of attack of $\pm 3°$ and then decreases for higher angles of attack. This type of variation was also obtained in reference 1. The broken line between the $\alpha = \pm 3°$ data at a Reynolds number of 2×10^6 is used to indicate that the true variation of the pressure coefficient in this region is unknown. As in reference 1, this behavior for the low Reynolds number may be associated with the movement of the boundary-layer-transition region with increasing angle of attack.

In an effort to gain an insight into the effect of boundary-layer development and body shape on the base-pressure coefficient, all the base-pressure coefficients for the five models are plotted as a function of angle of attack for a Reynolds number of 14×10^6 in figure 15. It is evident from figure 15 that for this particular Reynolds number the base-pressure coefficient is not altered significantly by the different boundary-layer developments or body shapes. In fact, the base-pressure coefficient does not vary more than ± 4 percent from a median line drawn through the data points.

2434

SUMMARY OF RESULTS

The aerodynamic load distributions of a series of five bodies having conical or slightly blunted noses and cylindrical afterbodies were investigated in the NACA Lewis 1- by 1-foot variable Reynolds number tunnel at a Mach number of 3.12. The results may be summarized as follows:

1. For zero angle of attack and a Reynolds number range of 2×10^6 to 14×10^6, linearized potential theory predicted the pressure distributions satisfactorily for the pointed bodies having large nose fineness ratios. The exact conical flow theory predicted the conical pressures well regardless of nose fineness ratio.

2. The total-drag coefficient for zero angle of attack and free transition increased with increasing Reynolds number until some Reynolds number between 2×10^6 and 8×10^6 was reached and then remained almost constant at a value of approximately 0.18.

3. For small angles of attack, the experimental pressure distributions due to angle of attack on the top and the bottom surfaces of a representative model were in satisfactory agreement with slender-body theory for all Reynolds numbers. The theoretical data obtained from Massachusetts Institute of Technology tables predicted the conical pressures well for all angles of attack.

4. The base-pressure coefficient for the higher Reynolds numbers decreased steadily as the angle of attack increased; for the low Reynolds number, however, the base-pressure coefficient first increased to a maximum near an angle of attack of $\pm 3^{\circ}$ and then decreased for larger angles of attack.

5. For the five models investigated at a Reynolds number of 14×10^6, the base-pressure coefficient did not vary more than ± 4 percent from a median curve.

Lewis Flight Propulsion Laboratory
    National Advisory Committee for Aeronautics
        Cleveland, Ohio

REFERENCES

1. Jack, John R., and Burgess, Warren C.: Aerodynamics of Slender Bodies at Mach Number of 3.12 and Reynolds Numbers from 2×10^6 to 15×10^6. I - Body of Revolution with Near-Parabolic Forebody and Cylindrical Afterbody. NACA RM E51H13, 1951.

2. Chapman, Dean R.: An Analysis of Base Pressure at Supersonic
   Velocities and Comparison with Experiment. NACA TN 2137, 1950.

3. Jack, John R.: Aerodynamic Characteristics of a Slender Cone-
   Cylinder Body of Revolution at a Mach Number of 3.85. NACA
   RM E51H17, 1951.

4. Luidens, Roger W., and Simon, Paul C.: Aerodynamic Characteristics
   of NACA RM-10 Missile in 8- by 6-Foot Supersonic Wind Tunnel at
   Mach Numbers from 1.49 to 1.98. I - Presentation and Analysis of
   Pressure Measurements (Stabilizing Fins Removed). NACA RM E50D10,
   1950.

5. von Kármán, Theodor, and Moore, Norton B.: Resistance of Slender
   Bodies Moving with Supersonic Velocities, with Special Reference
   to Projectiles. Trans. A.S.M.E., vol. 54, no. 23, Dec. 15, 1932,
   pp. 303-310.

6. Van Dyke, Milton D.: A Study of Second-Order Supersonic Flow Theory.
   NACA TN 2200, 1951.

7. Anon.: Tables of Supersonic Flow around Cones of Large Yaw. Tech.
   Rep. No. 5, Dept. Elec. Eng., M.I.T., 1949.

2434

TABLE I - LOCATION OF STATIC-PRESSURE ORIFICES FOR MODELS

Model 1

Axial station x (in.)	Meridian angle θ (deg)				
	0	22.5	45	87.5	90
1.00	x				x
2.00	x				x
3.38	x	x	x	x	x
4.84	x	x	x	x	x
5.09	x	x	x	x	x
5.50	x	x	x		x
6.00	x				x
6.50	x				x
7.00	x				x
7.75	x				x
8.50	x				x
10.00	x	x	x	x	x
11.50	x				x
13.00	x				x
14.50	x	x	x	x	x
16.00	x				x
17.50	x				x
19.00	x				x
20.50	x	x	x	x	x

Model 2[a]

Axial station x (in.)	Meridian angle θ (deg)				
	0	22.5	45	67.5	90
3.00	x*				x*
5.00	x	x	x	x	x
7.00	x*	*	*	*	x*
9.00	x				x
10.38	x*	x	x	x	x*
10.62	x	x	x	x	x
11.22	x*				x*
11.82	x				x
12.42	x*	x	x	x	x
13.02	x				x
13.50	x*				x
15.50	x*	x*	x*	x*	x*
17.50	x*				x
19.50	x*				x
20.50	x*	x*	x*	x*	x*

Model 3

Axial station x (in.)	Meridian angle θ (deg)				
	0	22.5	45	67.5	90
3.00	x				x
5.00	x	x	x	x	x
7.00	x				x
9.00	x				x
11.00	x				x
13.88	x	x	x	x	x
14.12	x	x	x	x	x
14.50	x				x
15.00	x				x
15.50	x				x
16.00	x				x
17.50	x	x	x	x	x
19.50	x				x
20.50	x	x	x	x	x

Model 4

Axial station x (in.)	Meridian angle θ (deg)				
	0	22.5	45	67.5	90
0.00	x				x
.12	x				x
.50	x				x
1.00	x				x
1.50	x				x
2.50	x				x
4.00	x	x	x	x	x
5.50	x				x
7.50	x	x	x	x	x
9.50	x				x
10.38	x	x	x	x	x
10.62	x	x	x	x	x
11.00	x				x
11.50	x				x
12.00	x				x
12.50	x				x
13.00	x				x
13.75	x				x
14.50	x				x
16.00	x	x	x	x	x
17.50	x				x
19.00	x				x
20.50	x	x	x	x	x

Model 5

Axial station x (in.)	Meridian angle θ (deg)				
	0	22.5	45	67.5	90
0.00	x				x
.12	x				x
.50	x				x
1.00	x				x
2.00	x				x
3.00	x				x
5.00	x	x	x	x	x
7.00	x				x
9.00	x	x	x	x	x
11.00	x				x
13.00	x				x
13.88	x	x	x	x	x
14.12	x	x	x	x	x
14.56	x				x
15.00	x				x
15.50	x				x
16.00	x				x
16.50	x				x
17.50	x	x	x	x	x
19.00	x				x
20.50	x	x	x	x	x

[a] Use of 0.035 in. I.D. tubing indicated by x and use of 0.048 in. I.D. tubing, by *.

11

TABLE II - PRESSURE COEFFICIENTS FOR MODEL 1 FOR TWO ANGLES OF ATTACK

AND REYNOLDS NUMBER OF 14×10^6

(a) Axial variation of pressure coefficient

Axial station x (in.)	Meridian angle θ (deg)		Axial station x (in.)	Meridian angle θ (deg)	
Angle of attack, α=3°			Angle of attack, α=6°[a]		
	0	180		0	180
1.00	0.1192	0.0475	1.00	0.1582	0.0286
2.00	.1221	.0507	2.00	.1651	.0279
3.38	.1192	.0537	3.38	.1717	.0304
4.84	.1218	.0507	4.84	.1722	.0318
5.09	-.0143	-.0390	5.09	.0100	-.0461
5.50	-.0172	-.0490	5.50	.0090	-.0568
6.00	-.0094	-.0288	6.00	.0306	-.0406
6.50	-.0104	-.0369	6.50	.0138	-.0443
7.00	-.0087	-.0312	7.00	.0149	-.0372
7.75	-.0070	-.0243	7.75	.0146	-.0281
8.50	-.0065	-.0187	8.50	.0132	-.0217
10.00	-.0033	-.0130	10.00	.0123	-.0166
11.50	-.0039	-.0117	11.50	.0118	-.0137
13.00	-.0072	-.0087	13.00	.0092	-.0134
14.50	-.0075	-.0100	14.50	.0073	-.0225
16.00	-.0098	-.0067	16.00	.0030	-.0110
17.50	-.0073	-.0041	17.50	.0015	-.0072
19.00	-.0028	-.0081	19.00	.0077	-.0137
20.50	-.0066	-.0086	20.50	.0020	-.0136

(b) Circumferential variation of pressure coefficient

Axial station x (in.)	Meridian angle θ (deg)						
Angle of attack, α=3°							
	22.5	45	67.5	90	112.5	135	157.5
3.38	0.1182	0.1143	0.1068	0.0939	0.0771	0.0617	0.0555
4.84	.1169	.1331	.1044	------	.0744	.0615	.0529
5.09	-.0152	-.0179	-.0227	-.0279	-.0336	-.0371	-.0399
10.00	-.0035	-.0091	-.0161	-.0203	-.0228	-.0193	-.0146
14.50	-.0065	-.0089	-.0119	-.0139	-.0140	-.0111	-.0094
20.50	.0040	-.0094	-.0137	-.0145	-.0134	-.0113	-.0107

Axial station x (in.)	Meridian angle θ (deg)						
Angle of attack, α=6°[a]							
	22.5	45	67.5	90	112.5	135	157.5
3.38	0.1730	0.1413	------	0.0805	0.0509	0.0336	0.0302
4.84	.1599	.1413	0.1082	------	.0502	.0361	.0317
5.09	.0071	-.0044	-.0197	-.0341	-.0449	-.0484	-.0487
10.00	.0060	-.0098	-.0272	-.0410	-.0466	-.0303	-.0212
14.50	.0022	-.0127	-.0321	-.0359	-.0278	-.0214	-.0224
20.50	-.0010	-.0167	-.0304	-.0305	-.0213	-.0198	-.0250

[a]Data for α=9° is not presented for model 1 because sporadic vibrations occurred for this condition.

TABLE III – PRESSURE COEFFICIENTS FOR MODEL 3 FOR TWO ANGLES OF ATTACK

AND REYNOLDS NUMBER OF 14×10⁶

(a) Axial variation of pressure coefficient

Angle of attack, α=3°			Angle of attack, α=9°		
Axial station x (in.)	Meridian angle θ (deg)		Axial station x (in.)	Meridian angle θ (deg)	
	0	180		0	180
3.00	0.0281	0.0043	3.00	0.0840	-0.0176
5.00	.0282	.0044	5.00	.0871	-.0136
9.00	.0296	.0092	9.00	.0852	-.0095
11.00	.0328	.0062	11.00	.0835	-.0125
13.88	.0297	.0043	13.88	.0888	-.0150
14.12	-.0059	-.0218	14.12	.0362	-.0462
14.50	-.0122	-.0261	14.50	.0328	-.0491
15.00	-.0119	-.0267	15.00	.0336	-.0471
15.50	-.0122	-.0243	15.50	.0329	-.0430
16.00	-.0109	-.0213	16.00	.0310	-.0377
17.50	-.0081	-.0104	17.50	.0278	-.0265
19.50	-.0071	-.0130	19.50	.0281	-.0310
20.50	-.0086	-.0119	20.50	.0251	-.0293

(b) Circumferential variation of pressure coefficient

Angle of attack, α=3°							
Axial station x (in.)	Meridian angle θ (deg)						
	22.5	45	67.5	90	112.5	135	157.5
5.00	0.0262	0.0196	0.0141	0.0078	0.0051	0.0038	0.0042
9.00	.0271	.0209	.0148	.0081	.0062	.0053	.0076
13.88	.0290	.0242	.0188	.0133	.0080	.0056	.0056
14.12	-.0071	-.0099	-.0139	-.0176	-.0242	-.0211	-.0208
17.50	-.0070	-.0140	-.0198	-.0237	-.0247	-.0212	-.0155
20.50	-.0076	-.0132	-.0186	-.0211	-.0185	-.0147	-.0123

Angle of attack, α=9°							
Axial station x (in.)	Meridian angle θ (deg)						
	22.5	45	67.5	90	112.5	135	157.5
5.00	0.0766	0.0376	0.0016	-0.0334	-0.0385	-0.0260	-0.0255
9.00	.0743	.0415	.0020	-.0386	-.0448	-.0230	-.0164
13.88	.0819	.0489	.0078	-.0325	-.0359	-.0233	-.0222
14.12	.0295	.0057	-.0267	-.0565	-.0577	-.0423	-.0447
17.50	.0233	-.0046	-.0392	-.0708	-.0559	-.0456	-.0394
20.50	.0197	-.0099	-.0462	-.0762	-.0443	-.0441	-.0452

TABLE IV - PRESSURE COEFFICIENTS FOR MODEL 4 FOR TWO ANGLES OF ATTACK

AND REYNOLDS NUMBER OF 14×10^6

(a) Axial variation of pressure coefficient

Angle of attack, α=3°			Angle of attack, α=9°		
Axial station x (in.)	Meridian angle θ (deg)		Axial station x (in.)	Meridian angle θ (deg)	
	0	180		0	180
0.00	1.7250	1.7250	0.00	1.6880	1.6880
.12	.1885	.0901	.12	.3210	.0179
.50	.0327	-.0137	.50	.0942	-.0382
1.00	.0229	-.0124	1.00	.0778	-.0254
1.50	.0213	-.0103	1.50	.0770	-.0177
2.50	.0218	-.0062	2.50	.0835	-.0119
4.00	.0234	.0002	4.00	.0899	-.0111
5.50	.0272	.0026	5.50	.0907	-.0103
7.50	.0290	.0077	7.50	.0884	-.0104
9.50	.0338	.0095	9.50	.0903	-.0109
10.38	.0342	.0063	10.38	.0893	-.0143
10.62	-.0042	-.0183	10.62	.0371	-.0417
11.00	-.0077	-.0211	11.00	.0340	-.0445
11.50	-.0080	-.0226	11.50	.0339	-.0442
12.00	-.0076	-.0214	12.00	.0344	-.0415
12.50	-.0070	-.0197	12.50	.0359	-.0369
13.00	-.0072	-.0183	13.00	.0350	-.0361
13.75	-.0080	-.0175	13.75	.0345	-.0327
14.50	-.0062	-.0153	14.50	.0310	-.0315
16.00	-.0086	-.0113	16.00	.0247	-.0298
17.50	-.0068	-.0065	17.50	.0229	-.0250
19.00	-.0014	-.0095	19.00	.0292	-.0233
20.50	-.0066	-.0088	20.50	.0247	-.0211

(b) Circumferential variation of pressure coefficient

Angle of attack, α=3°								Angle of attack, α=9°							
Axial station x (in.)	Meridian angle θ (deg)							Axial station x (in.)	Meridian angle θ (deg)						
	22.5	45	67.5	90	112.5	135	157.5		22.5	45	67.5	90	112.5	135	157.5
4.00	0.0223	0.0167	0.0098	0.0039	-0.0011	-0.0030	-0.0010	4.00	0.0790	0.0407	-0.0043	-0.0404	-0.0369	-0.0354	-0.0310
7.50	.0279	.0251	.0158	.0083	.0047	.0053	.0071	7.50	.0789	.0470	-.0001	-.0393	-.0479	-.0211	-.0252
10.38	.0325	.0263	.0184	.0123	.0088	.0069	10.38	.0777	.0442	-.0004	-.0371	-.0496	-.0212	-.0166
10.62	-.0059	-.0103	-.0154	-.0197	-.0238	-.0224	-.0195	10.68	.0273	.0007	-.0327	-.0606	-.0705	-.0443	-.0398
16.00	-.0072	-.0087	-.0084	-.0128	-.0185	-.0135	-.0108	16.00	.0202	-.0075	-.0413	-.0698	-.0465	-.0438	-.0390
20.50	-.0053	-.0112	-.0147	-.0161	-.0151	-.0127	-.0100	20.50	.0173	-.0150	-.0506	-.0485	-.0363	-.0388	-.0518

TABLE V - PRESSURE COEFFICIENTS FOR MODEL 5 FOR TWO ANGLES OF ATTACK

AND REYNOLDS NUMBER OF 14×10^6

(a) Axial variation of pressure coefficient

Angle of attack, α=3°			Angle of attack, α=9°		
Axial station x (in.)	Meridian angle θ (deg)		Axial station x (in.)	Meridian angle θ (deg)	
	0	180		0	180
0.00	1.7080	1.7080	0.00	1.7090	1.7090
.12	.0810	.0163	.12	.1722	-.0375
.50	.0184	-.0176	.50	.0734	-.0355
1.00	.0129	-.0163	1.00	.0621	-.0280
2.00	.0169	-.0091	2.00	.0832	-.0159
3.00	.0173	-.0048	3.00	.0678	-.0150
5.00	.0197	.0013	5.00	.0758	-.0168
7.00	.0221	.0039	7.00	.0744	-.0151
9.00	.0228	.0056	9.00	.0739	-.0157
11.00	.0263	.0024	11.00	.0737	-.0167
13.00	.0236	.0018	13.00	.0758	-.0189
13.88	.0231	0.0000	13.88	.0805	-.0190
14.12	-.0073	-.0190	14.12	.0338	-.0433
14.55	-.0085	-.0203	14.55	.0328	-.0447
15.00	-.0078	-.0206	15.00	.0533	-.0429
15.50	-.0084	-.0195	15.50	.0323	-.0400
16.00	-.0103	-.0186	16.00	.0280	-.0366
16.50	-.0086	-.0156	16.50	.0275	-.0321
17.50	-.0057	-.0102	17.50	.0278	-.0315
19.00	-.0024	-.0125	19.00	.0273	-.0312
20.50	-.0073	-.0116	20.50	.0280	-.-241

(b) Circumferential variation of pressure coefficient

Angle of attack, α=3°							
Axial station x (in.)	Meridian angle θ (deg)						
	22.5	45	67.5	90	112.5	135	157.5
5.00	0.0189	0.0141	0.0078	0.0026	-0.0005	-0.0006	0.0013
9.00	.0220	.0170	.0104	.0056	.0024	.0029	.0048
13.88	.0245	.0219	.0168	.0099	.0033	.0011	.0009
14.12	-.0065	-.0084	-.0117	-.0162	-.0194	-.0197	-.0183
17.50	-.0051	-.0127	-.0165	-.0206	-.0227	-.0195	-.0137
20.50	-.0063	-.0113	-.0166	-.0196	-.0179	-.0149	-.0127

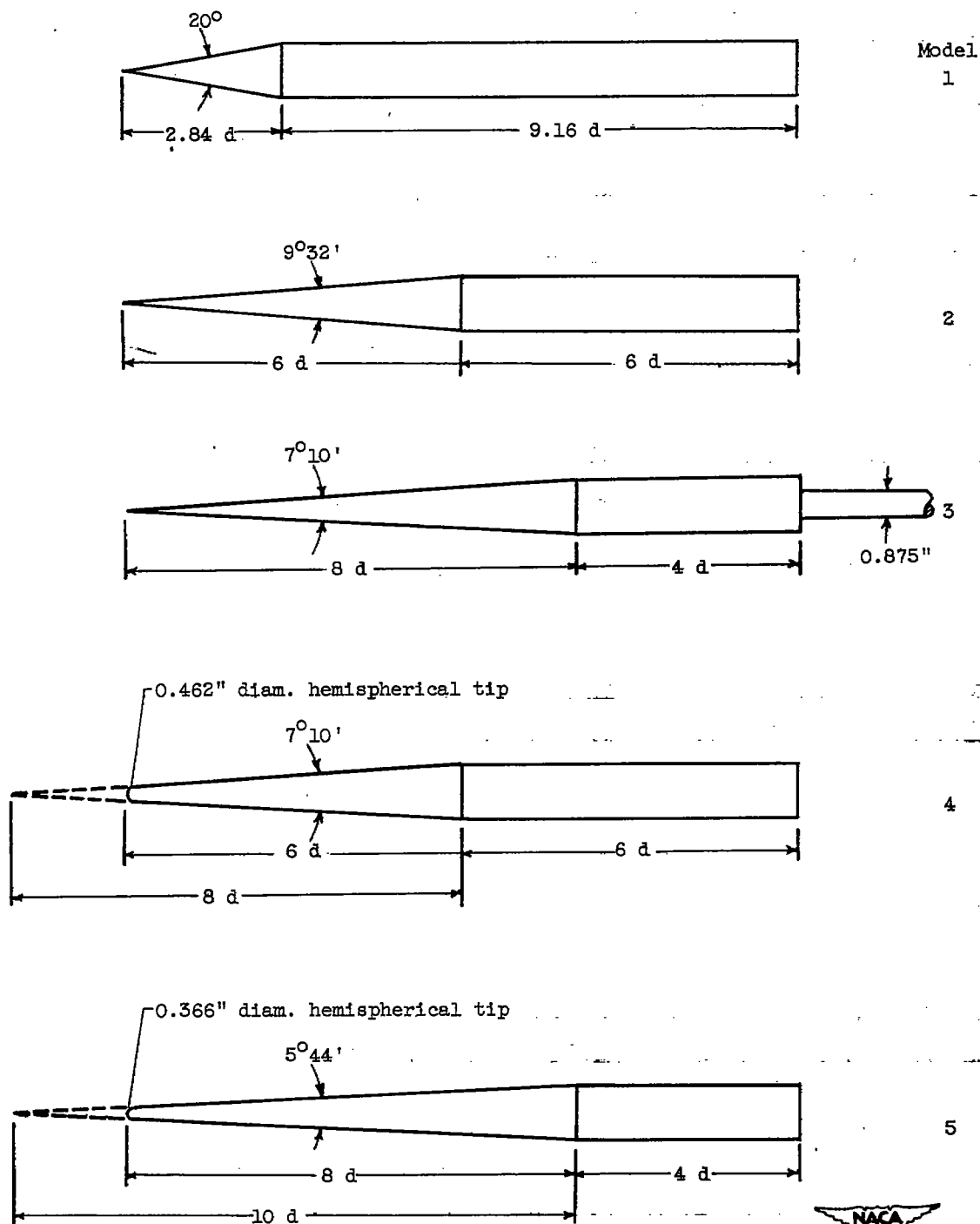| Angle of attack, α=9°							
Axial station x (in.)	Meridian angle θ (deg)						
	22.5	45	67.5	90	112.5	135	157.5
5.00	0.0630	0.0284	-0.0127	-0.0362	-0.0398	-0.0248	-0.0260
9.00	.0631	.0312	-.0093	-.0445	-.0396	-.0235	-.0224
13.88	.0671	.0354	-.0080	-.0437	-.0406	-.0254	-.0252
14.12	.0271	.0015	-.0325	-.0621	-.0617	-.0402	-.0408
17.50	.0227	-.0083	-.0431	-.0711	-.0540	-.0429	-.0375
20.50	.0184	-.0123	-.0492	-.0637	-.0426	-.0407	-.0413

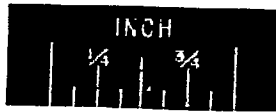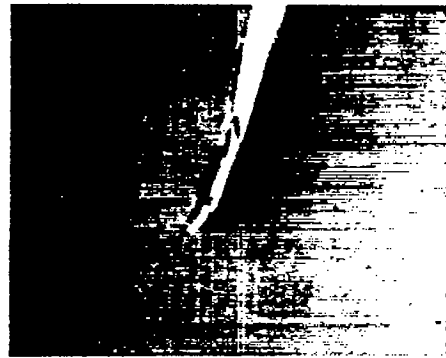Figure 1. - Schematic drawing of models.   Maximum body diameter d, 1.75 inches.

2434

Figure 2. - Probe used to obtain boundary-layer data at zero angle of attack.

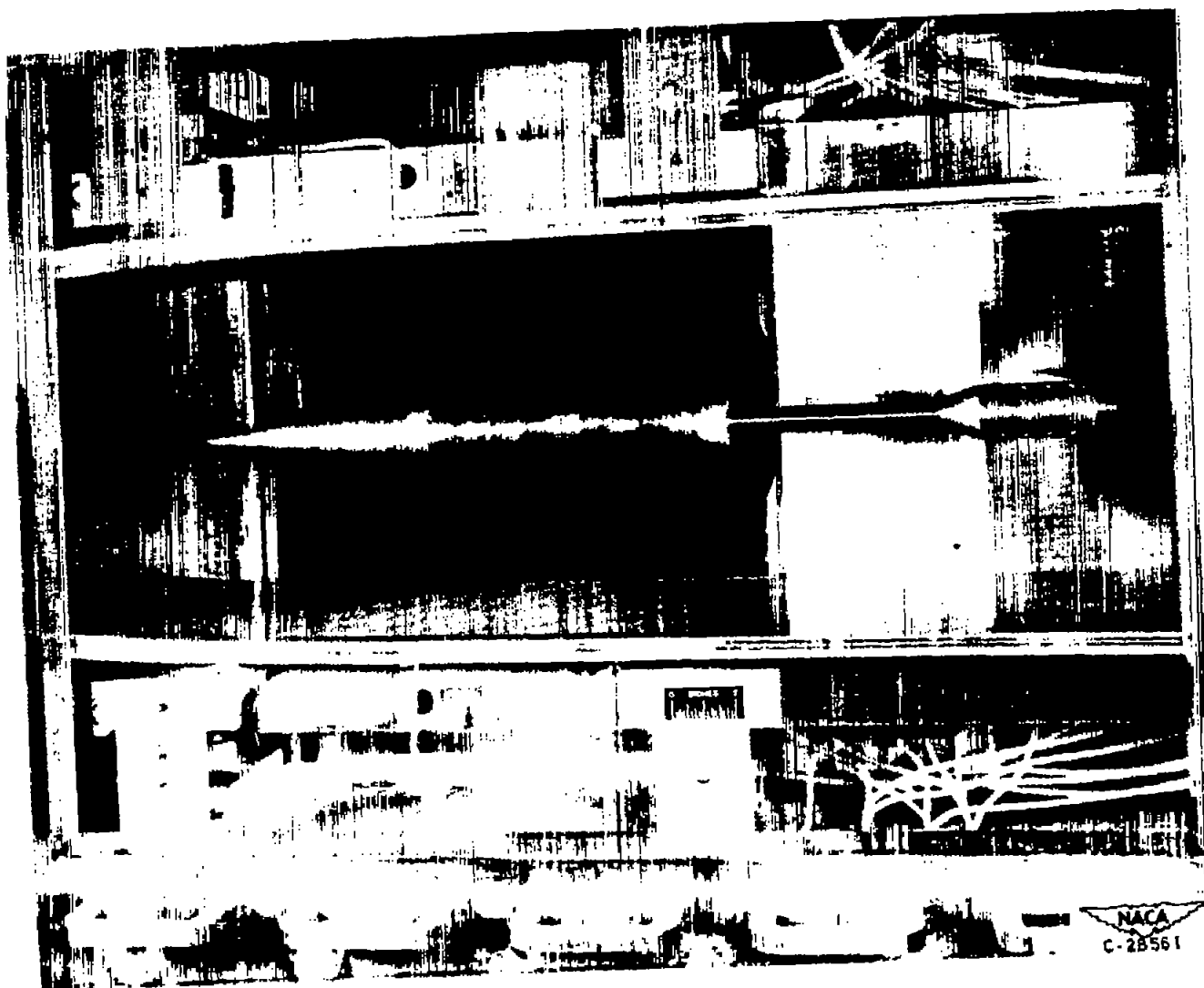Figure 3. - Representative model 2 installed in Lewis 1- by 1-foot supersonic wind tunnel.
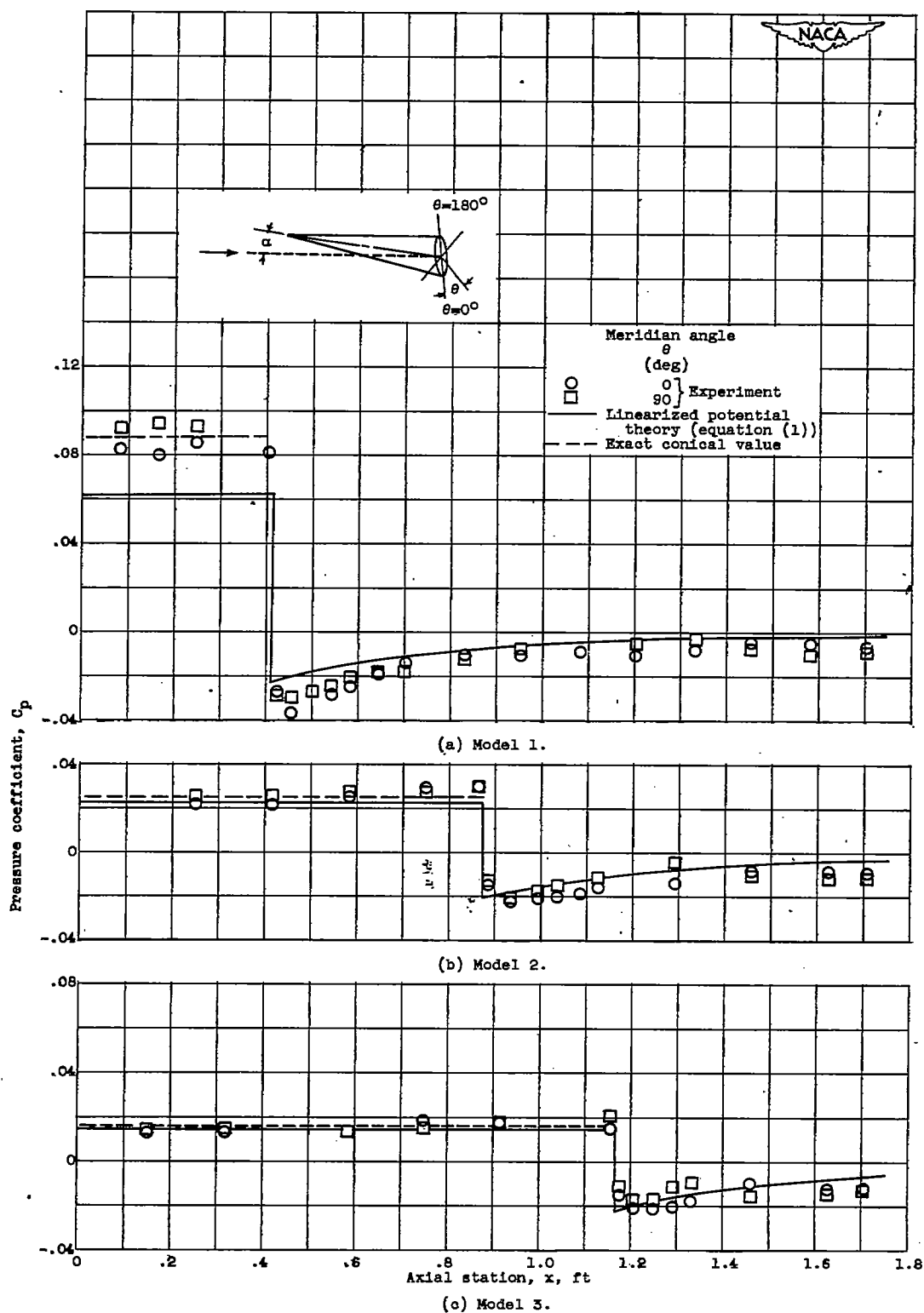
(a) Model 1.

(b) Model 2.

(c) Model 3.

Figure 4. - Experimental and theoretical axial variation of pressure coefficient for model at zero angle of attack and Reynolds number of 14×10^6.
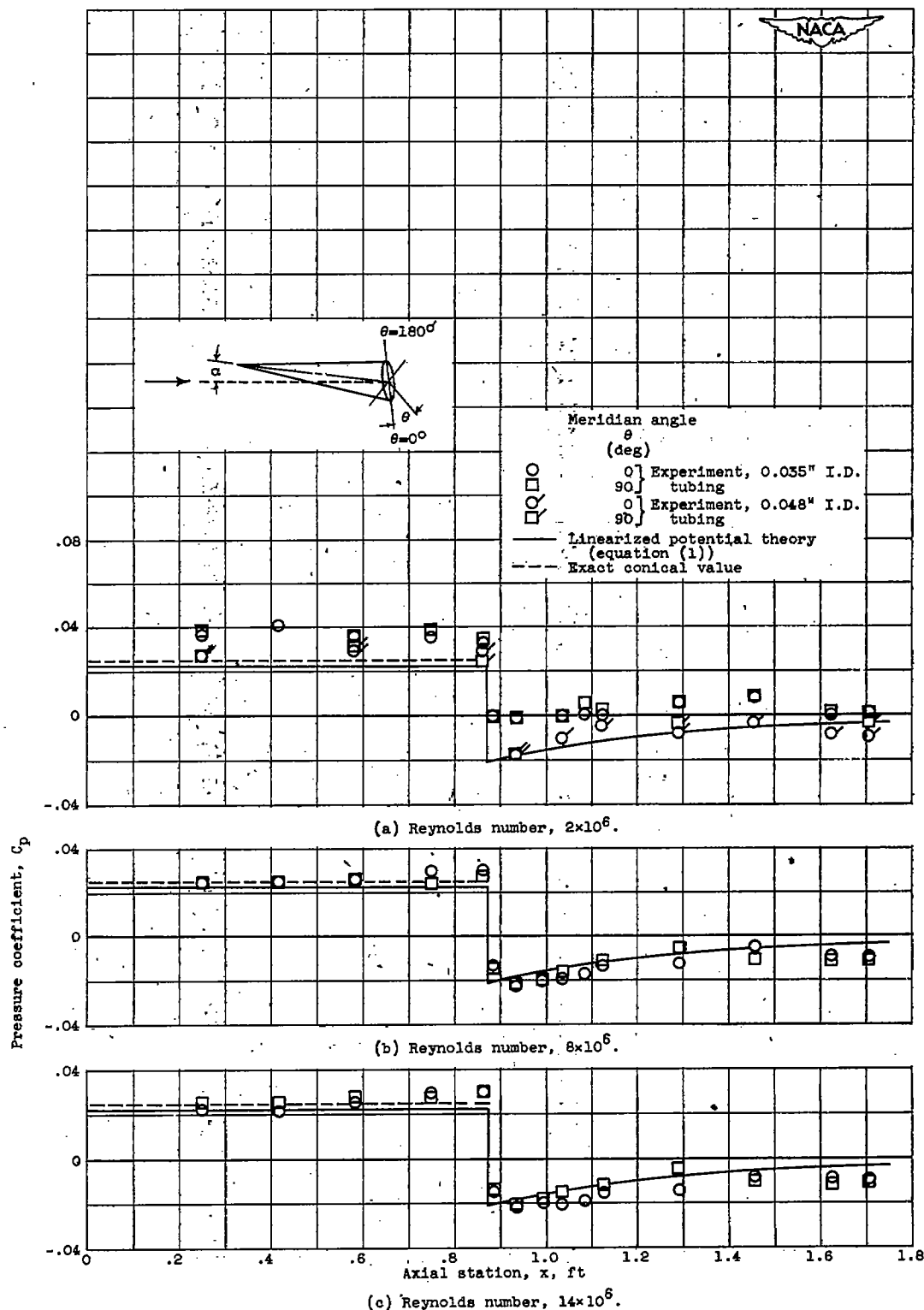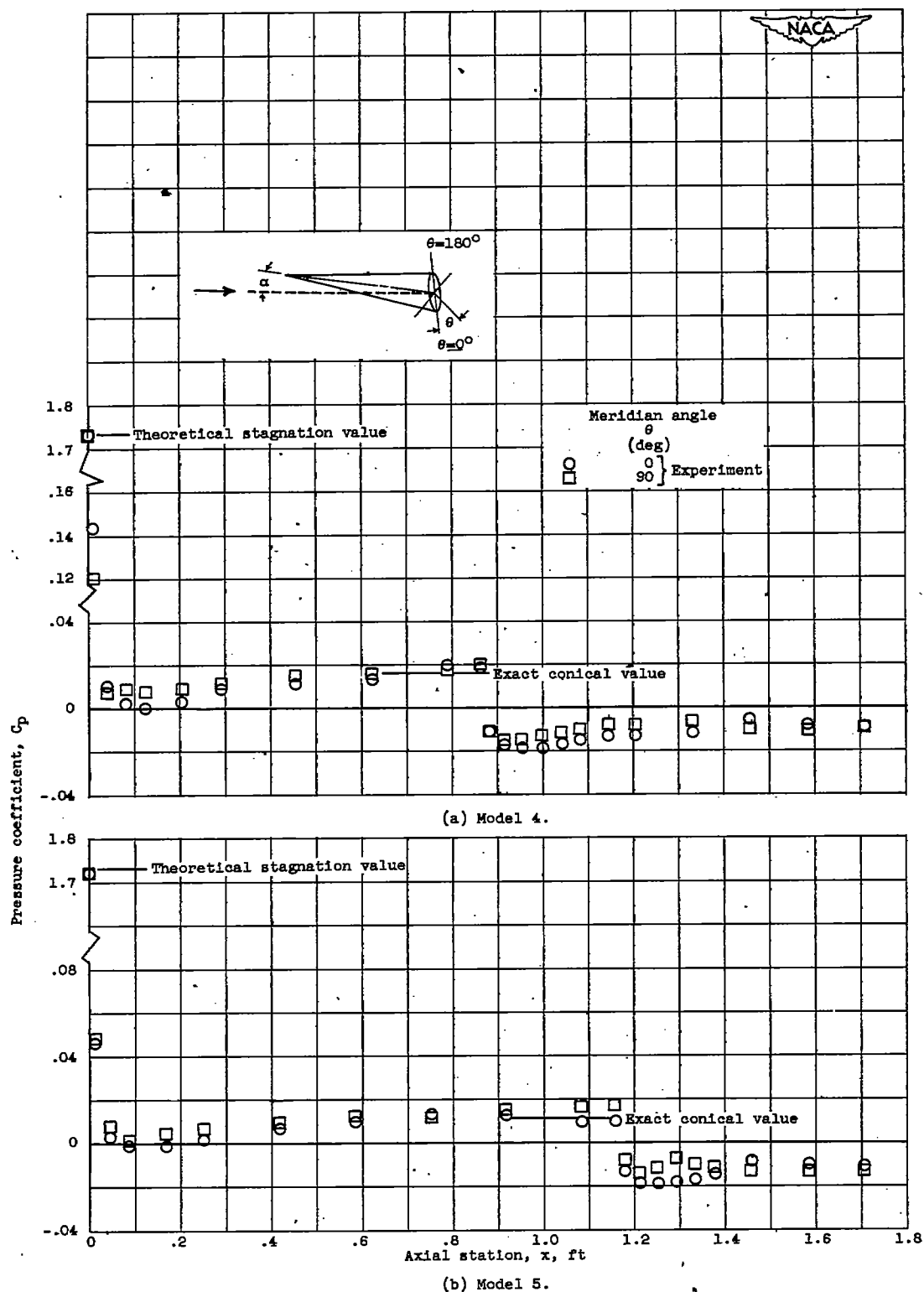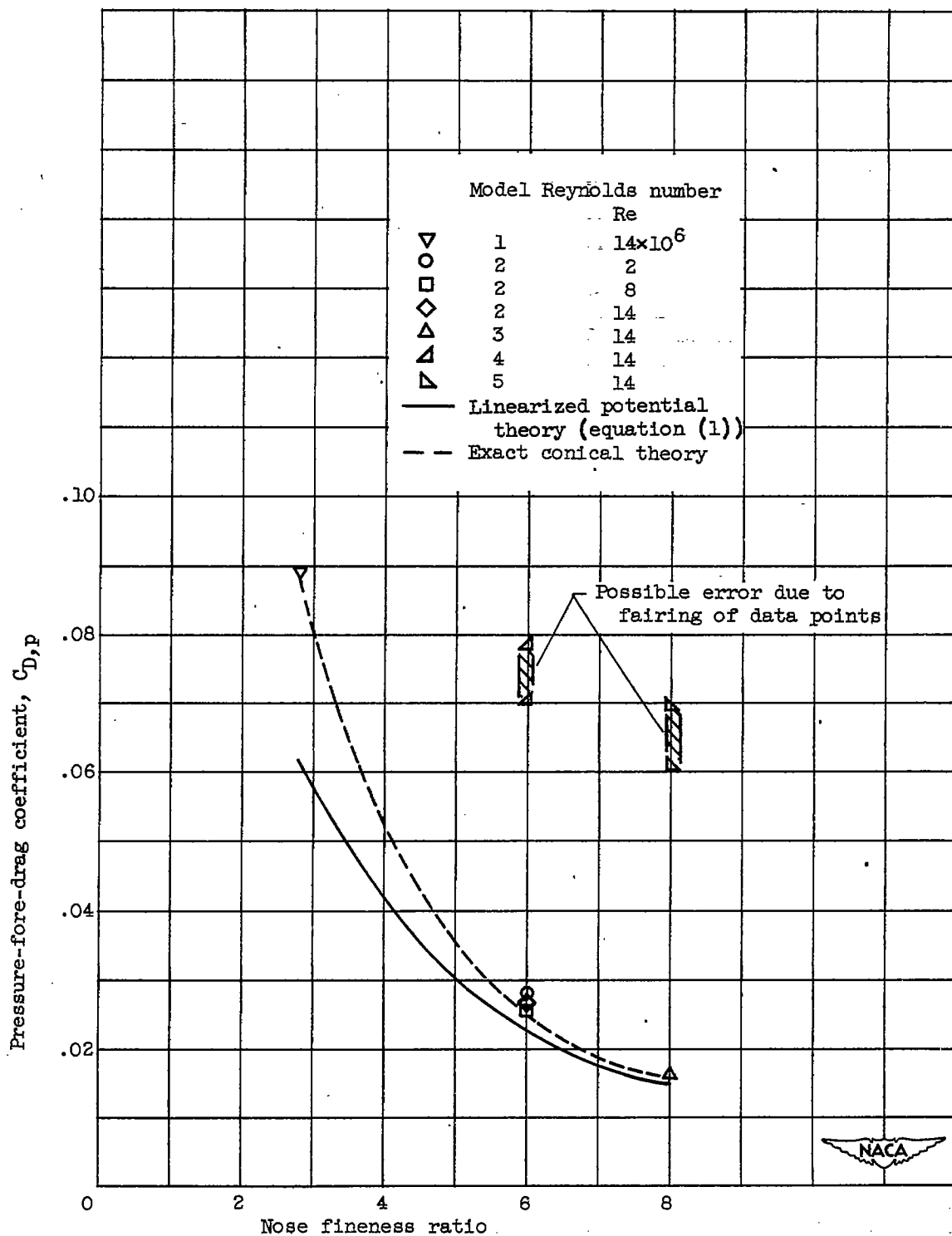
(a) Reynolds number, 2×10^6.

(b) Reynolds number, 8×10^6.

(c) Reynolds number, 14×10^6.

Figure 5. - Experimental and theoretical axial variation of pressure coefficient for representative model at zero angle of attack.

2434

(a) Model 4.

(b) Model 5.

Figure 6. - Experimental axial variation of pressure coefficient for blunt-nosed body at zero angle of attack and Reynolds number of 14×10^6.

Figure 7. - Experimental and theoretical variation of pressure-fore-drag coefficient with nose fineness ratio.

2434
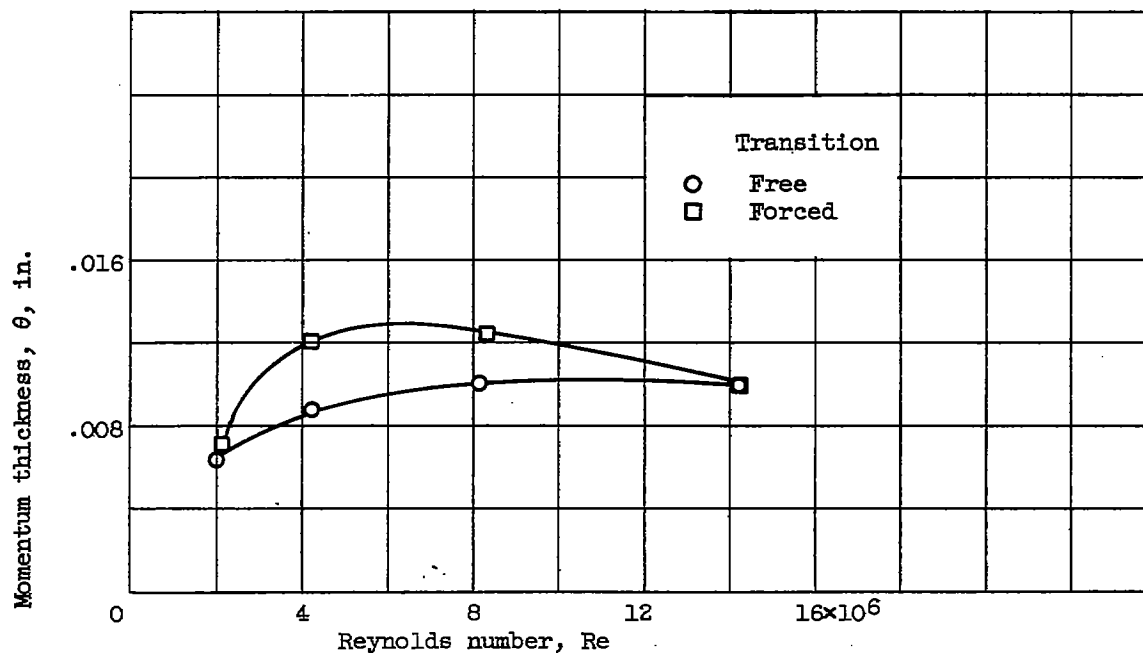
Figure 8. - Variation of momentum thickness with Reynolds
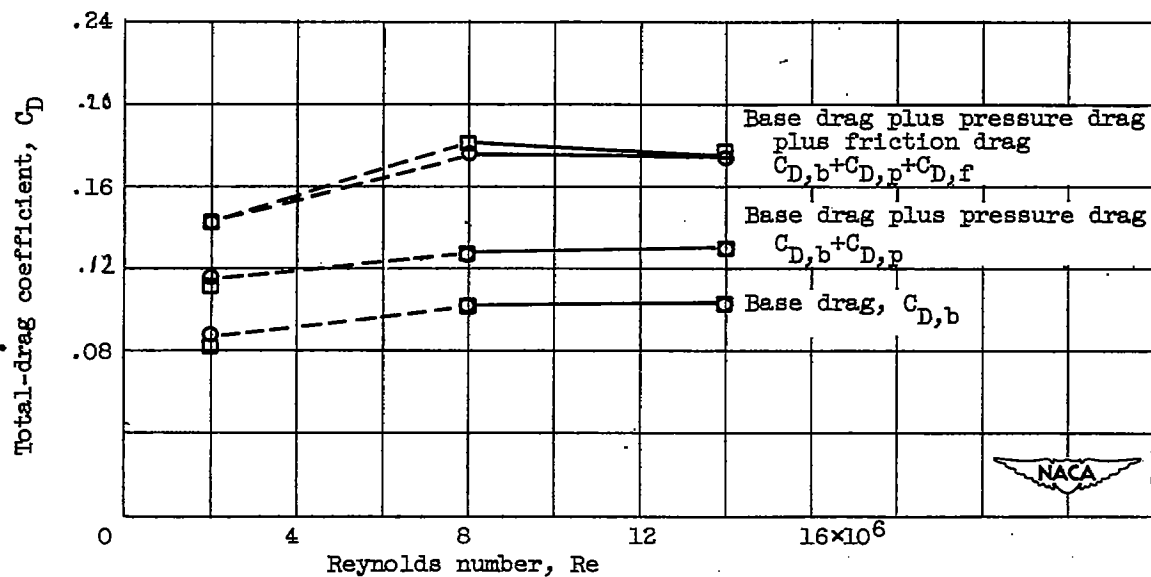number for zero angle of attack.

Figure 9. - Variation of total-drag coefficient with Reynolds number for
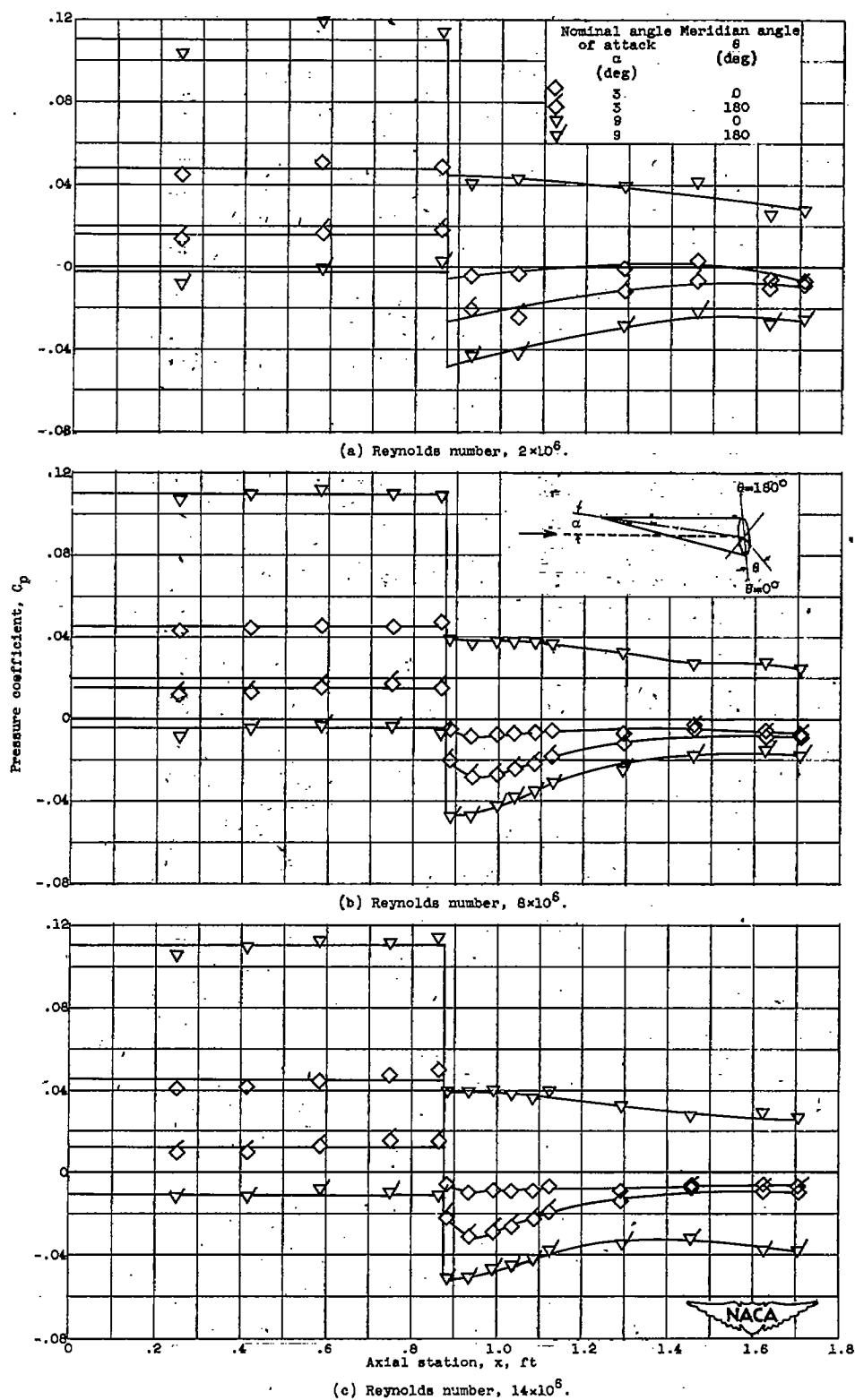zero angle of attack.

(a) Reynolds number, 2×10^6.

(b) Reynolds number, 8×10^6.

(c) Reynolds number, 14×10^6.

Figure 10. - Experimental axial variation of pressure coefficient for two angles of attack.

(a) Reynolds number, 2×10^6.

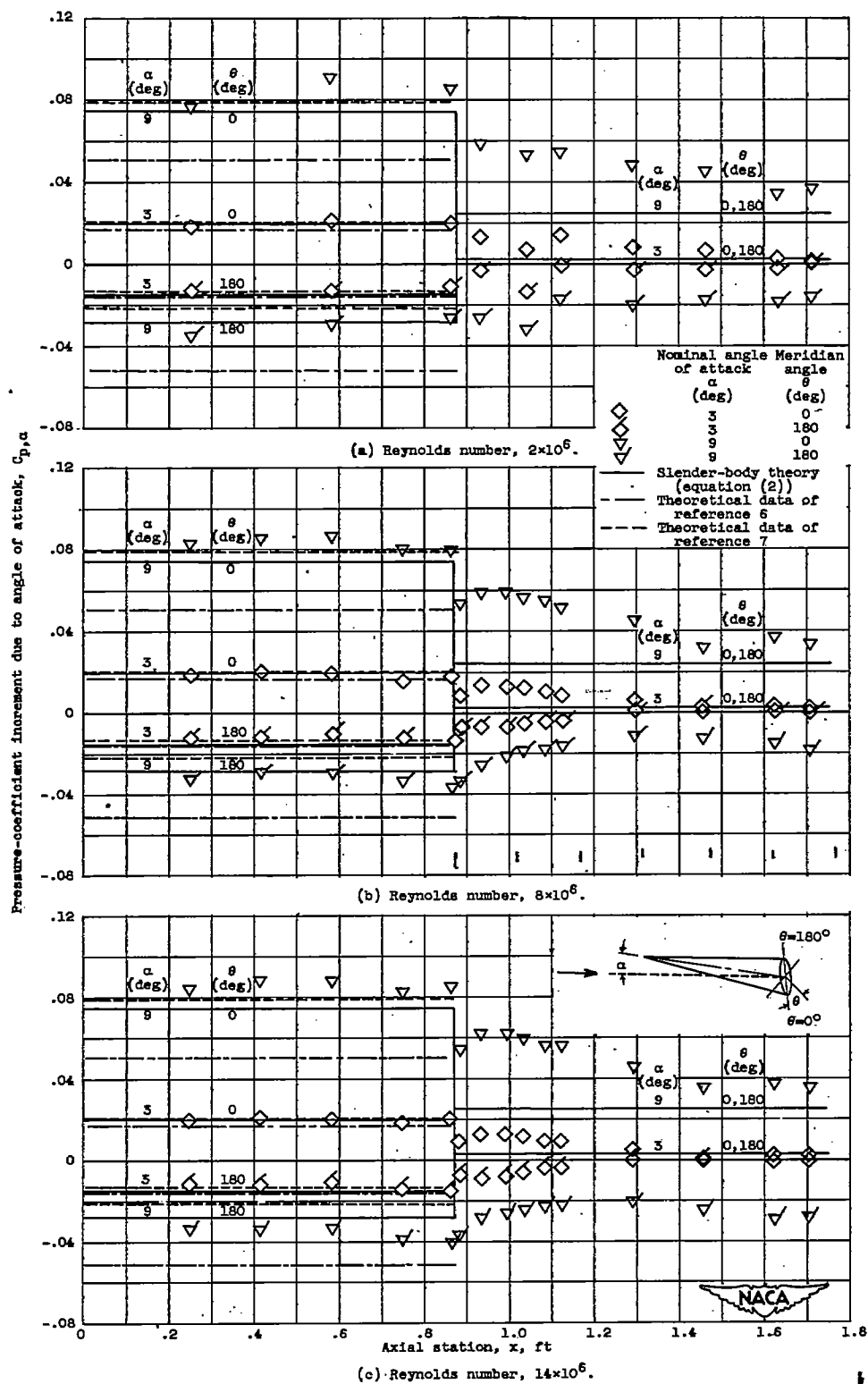(b) Reynolds number, 8×10^6.

(c) Reynolds number, 14×10^6.

Figure 11. - Experimental and theoretical axial variation of pressure-coefficient increment due to angle of attack.
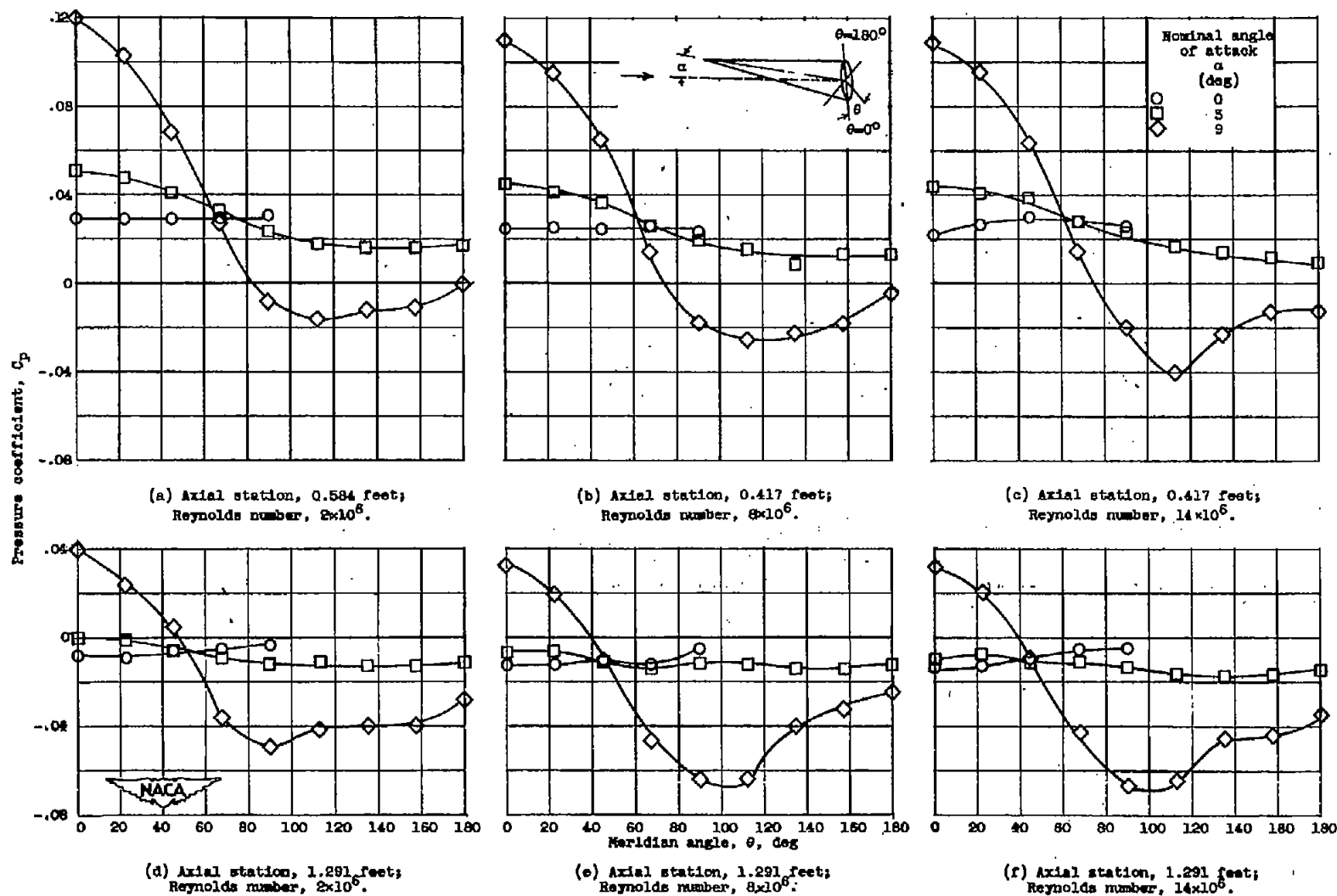
Model 2

(a) Axial station, 0.584 feet;
Reynolds number, 2×10⁶.

(b) Axial station, 0.417 feet;
Reynolds number, 8×10⁶.

(c) Axial station, 0.417 feet;
Reynolds number, 14×10⁶.

(d) Axial station, 1.291 feet;
Reynolds number, 2×10⁶.

(e) Axial station, 1.291 feet;
Reynolds number, 8×10⁶.

(f) Axial station, 1.291 feet;
Reynolds number, 14×10⁶.

Figure 12. - Experimental variation of pressure coefficient with meridian angle for given axial stations.

(g) Axial station, 1.708 feet;
Reynolds number, 2×10⁶.

(h) Axial station, 1.708 feet;
Reynolds number, 8×10⁶.

(i) Axial station, 1.708 feet;
Reynolds number, 14×10⁶.
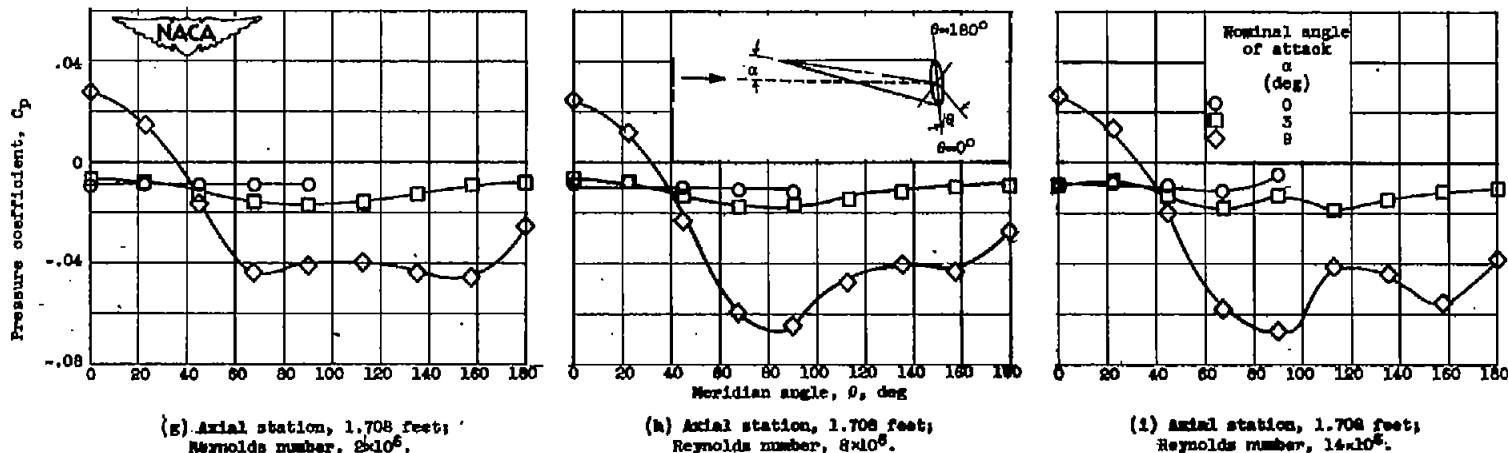
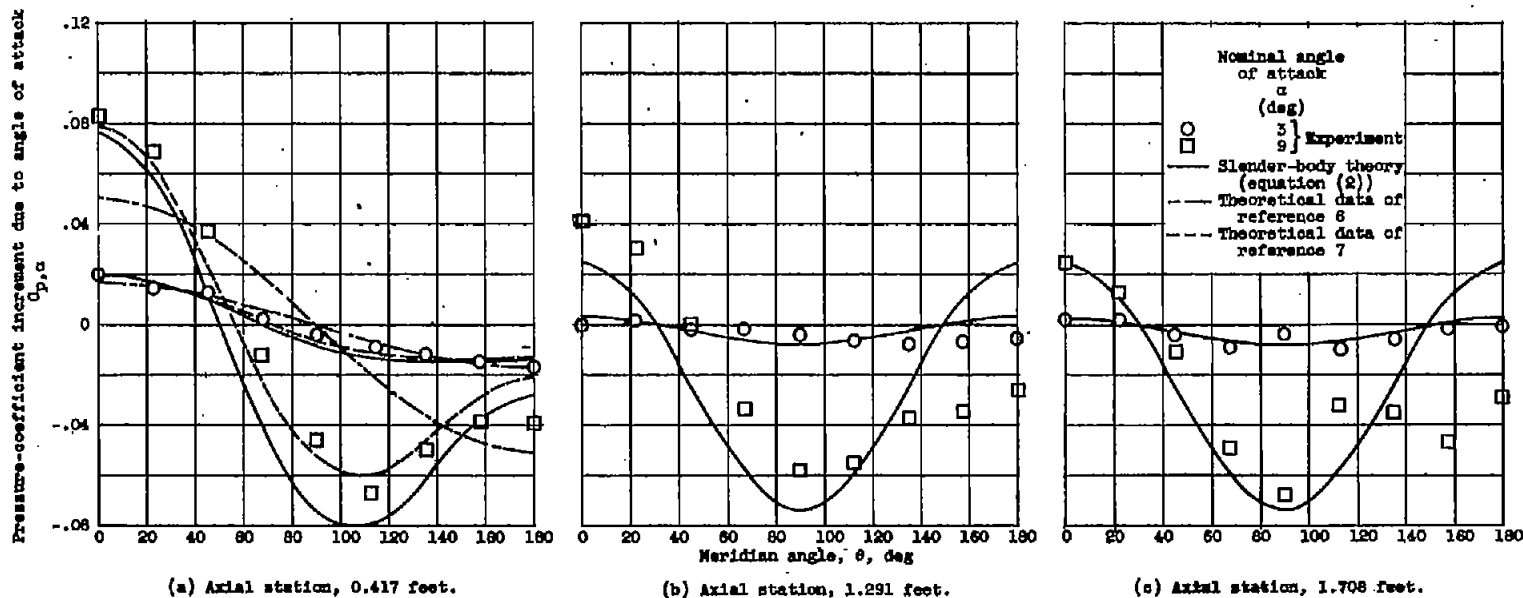Figure 12. - Concluded. Experimental variation of pressure coefficient with meridian angle for given axial stations.

(a) Axial station, 0.417 feet.

(b) Axial station, 1.291 feet.

(c) Axial station, 1.708 feet.

Figure 13. - Theoretical and experimental variation of pressure-coefficient increment due to angle of attack with angular position for two angles of attack and Reynolds number of 14×10⁶.
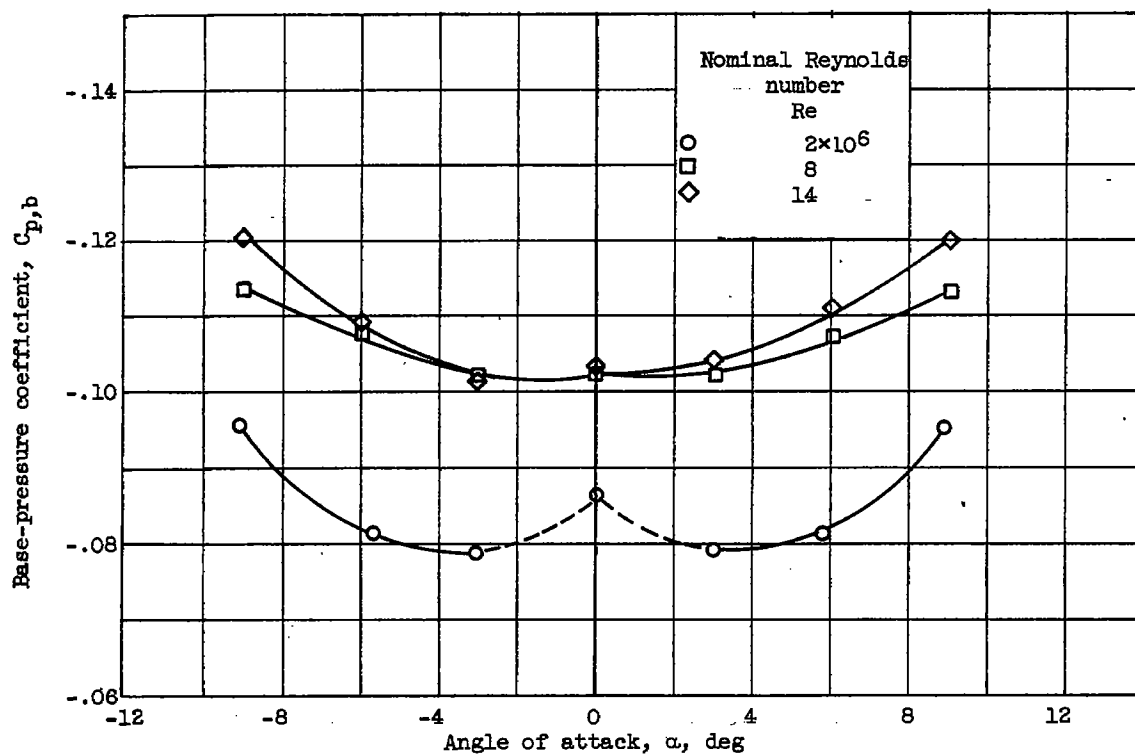
Figure 14. - Variation of base-pressure coefficient with angle of attack for Reynolds numbers of 2×10^6, 8×10^6, and 14×10^6.
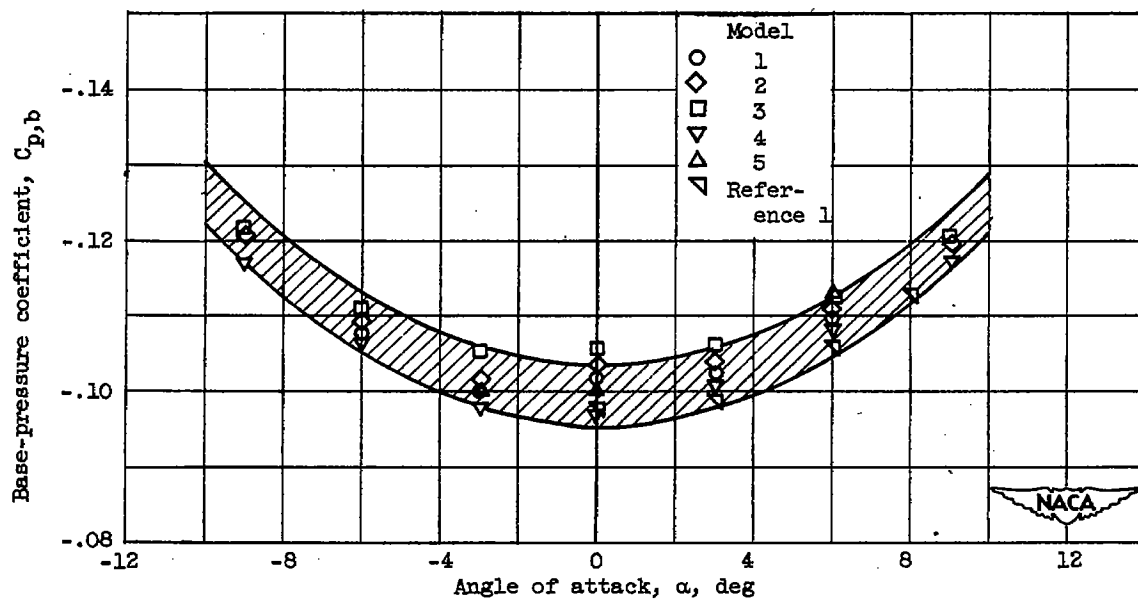

Figure 15. - Variation of base-pressure coefficient with angle of attack for five models at Mach number of 3.12 and Reynolds number of 14×10^6.